Competition between the antiferromagnetic charge-ordered and ferromagnetic states in doped manganites

Y. Moritomo
CIRSE, Nagoya University, Nagoya 464-8601, Japan
and PRESTO, JST, Tokyo 102, Japan
(Received 14 June 1999)

Structural and magnetic properties are systematically investigated for filling- and structure-controlled manganites $(La_{1-z}Nd_z)_{1-x}Ca_xMnO_3$ ($0.35 \leqslant x \leqslant 0.50$, $0.0 \leqslant z \leqslant 1.0$). The ground state at a fixed x value was found to change from ferromagnetic metallic (FM) to charge-ordered insulating (CO) states with increase of z. We have found suppressed ferromagnetic moment ($\sim 0.5\mu_B - 2.5\mu_B$ at 1 T) at 10 K in the vicinity of the FM-CO phase boundary, and have ascribed it to the phase separation (PS) into the FM and CO states. The PS region spreads out around the FM-CO phase boundary in the ground-state phase diagram. [S0163-1829(99)04634-2]

I. INTRODUCTION

The doped manganites, $R_{1-x}Ca_xMnO_3$, where R is a trivalent rare-earth metal, have the distorted perovskite structure with three-dimensional networks of the MnO_6 octahedra. Their generic behavior of paramagnetic-to-ferromagnetic transition is understood within the framework of double-exchange theory,[1–3] which includes only the transfer integral t of the e_g electrons and the on-site exchange interaction (Hund's rule coupling J_H) between the itinerant e_g electrons and localized t_{2g} spins ($S=3/2$). We need to include additional effects, e.g., electron-phonon coupling, however, to understand the insulating behavior in the paramagnetic state.[4]

Extensive study on the perovskite-type doped manganites begins to reveal the unusual microscopical structures of spin-, charge-, and orbital-ordered state.[5–7] Among them, $La_{1/2}Ca_{1/2}MnO_3$ (nominal hole concentration $x=0.5$), which is a ferromagnet [T_{CO} ($\sim$140–190 K) $\leqslant T \leqslant T_C$ ($=230$ K)] but is transferred into an antiferromagnetic charge-ordered (CO) insulator below T_C,[8] is most intensively studied. Electron-diffraction measurement[7] as well as ^{139}La and ^{55}Mn NMR measurements[6] have revealed a coexistence of the ferromagnetic metallic (FM) and antiferromagnetic CO states. Such a coexistence of the FM and CO phases, or the electronic phase separation (PS), is a new aspect of the doped manganites.[9,10] Similar PS effects are observed at lower-x or higher-x regions. For example, Ibarra *et al.*[11] have performed a neutron-diffraction experiment on $(La_{0.5}Nd_{0.5})_{1-x}Ca_xMnO_3$ ($x=0.33$) and revealed the coexistence of the antiferromagnetic CO component in the FM phase. Liu *et al.*[12] have investigated optical spectra on $Bi_{1-x}Ca_xMnO_3$ ($x=0.74$ and 0.82) and proposed a coexistence of the ferromagnetic and antiferromagnetic domains ($160\ \text{K} \leqslant T \leqslant 210\ \text{K}$). The aim of the present work is to clarify the PS region in the ground-state phase diagram of $(La_{1-z}Nd_z)_{1-x}Ca_xMnO_3$.

The charge-ordering transition of doped manganites usually accompanies an antiferromagnetic transition with the so-called CE-type[14] structure, while the FM state is half metallic with $\sim 3\mu_B - 4\mu_B$ moment per Mn site. Then, careful and systematic analysis of the magnetic properties will give us significant information on the competition between the FM and CO states. In this paper, we have derived a ground-state phase diagram of filling- and structure-controlled manganites $(La_{1-z}Nd_z)_{1-x}Ca_xMnO_3$ ($0.35 \leqslant x \leqslant 0.50$, $0.0 \leqslant z \leqslant 1.0$). It is well established that the CO state is amenable to the external pressure or chemical pressure,[13] both of which enhances itinerancy of the e_g carriers and hence the FM state. Here, we can effectively reduce the one-electron bandwidth W by increasing z (*chemical pressure*).[15] In the vicinity of the FM-CO phase boundary, a suppressed ferromagnetic moment ($\sim 0.5\mu_B - 2.5\mu_B$ at 1 T) is observed at 10 K due to the PS effect. The thus obtained phase diagram should be useful for global comprehension of the physical properties of doped manganites.

II. EXPERIMENTAL

The ceramics compounds, $(La_{1-z}Nd_z)_{1-x}Ca_xMnO_3$, were synthesized by solid-state reaction in air atmosphere. A stoichiometric mixture of commercial La_2O_3, Nd_2O_3, $CaCO_3$, and Mn_3O_4 powder was well ground and calcined twice at 1350 °C for 24 h. Then, the resulting powder was pressed into a disk with a size of 20 mm$\phi \times 4$ mm and sintered at 1350 °C for 24 h. Powder x-ray-diffraction measurements at room temperature and Rietveld analysis[16] indicate that all the investigated compounds were single phase without detectable impurity. The crystal symmetry is orthorhombic ($Pbnm$; $Z=4$).

The thus obtained lattice constants at room temperature, a, b, and $c/\sqrt{2}$, are plotted in Fig. 1. In every doping level, b and c decrease by $\sim 1\%$ from La compound ($z=0.0$) to Nd compound ($z=1.0$), reflecting the reduced averaged ionic radius of the perovskite A site. By contrast, a shows negligible z dependence.

III. RESULTS AND DISCUSSION

A. Suppressed magnetization due to phase separation

We show in Fig. 2 the magnetization curves for $La_{1/2}Ca_{1/2}MnO_3$ at various temperatures. The inset shows

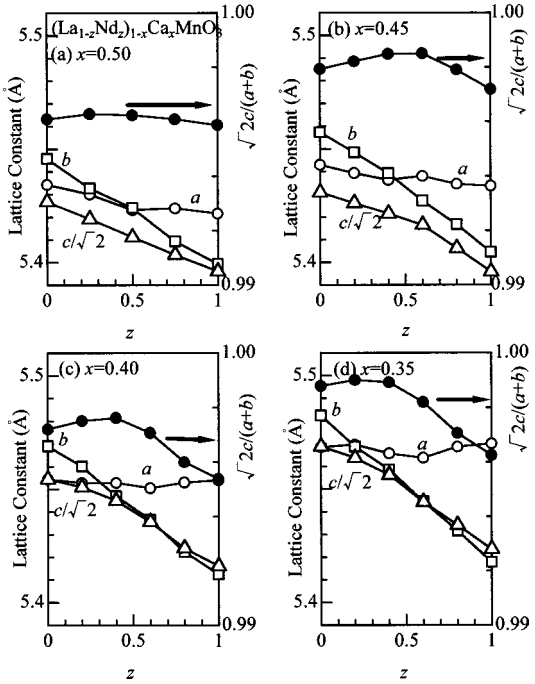

FIG. 1. Nd concentration dependence of lattice constants (open symbols) at room temperature for $(La_{1-z}Nd_z)_{1-x}Ca_xMnO_3$: (a) $x=0.50$, (b) $x=0.45$, (c) $x=0.40$, and (d) $x=0.35$. Filled circles are relative lattice constants of c.

temperature variation of magnetization M measured under a field of $\mu_0 H=0.5$ T after cooling down to 5 K in the zero field (ZFC), using a superconducting quantum interference device (SQUID) magnetometer. A prominent thermal hysteresis is observed in the temperature range of 140–220 K, consistently with the previous report.[8,17] The M-H curve in the FM phase ($T_{CO} \leqslant T \leqslant T_C$; broken curve) steeply rises

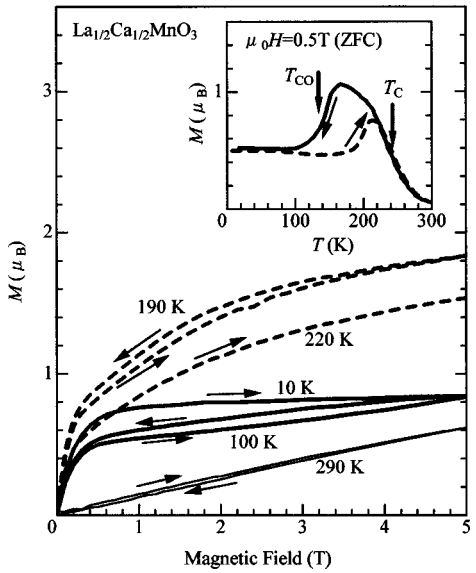

FIG. 2. Magnetization curves at various temperatures for $La_{1/2}Ca_{1/2}MnO_3$. These curves are measured after annealing at 300 K in zero field. The inset shows temperature variation of magnetization M. M was measured after cooling down to 5 K in zero field (ZFC). T_C and T_{CO} represent the Curie and charge-ordering temperatures, respectively.

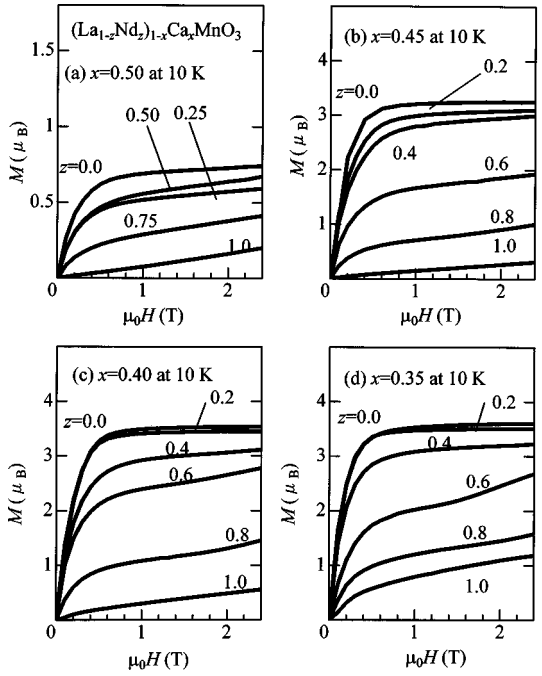

FIG. 3. Nd concentration dependence of magnetization curves at 10 K for $(La_{1-z}Nd_z)_{1-x}Ca_xMnO_3$: (a) $x=0.50$, (b) $x=0.45$, (c) $x=0.40$, and (d) $x=0.35$.

with the applied field, making a sharp contrast with the linear increase in the paramagnetic phase ($T \geqslant T_C$; thin curve). Surprisingly, the M-H curves in the antiferromagnetic CO phase ($T \leqslant T_{CO}$; thick curve) is reminiscent of ferromagnetism, although the absolute magnitude is fairly suppressed.

Such a ferromagnetic component (20– 30 % of the ideal value) should be due to the coexisting FM domains, or the PS effect, which has been confirmed by electron microscope.[7] With increase of temperature, size of the CO domains decreases from 50–60 nm at 95 K ($\leqslant T_{CO}$) to 20–30 nm at 142 K ($\geqslant T_{CO}$). The magnetization curve (broken curve in Fig. 2) in the FM phase is typical of a ferromagnet, but the absolute magnitude of M is rather small ($\sim 1.8\mu_B$ at 5 T and at 190 K) due to the coexistence of the nonferromagnetic CO domains. Recently, Moritomo *et al.*[18] have reported a similar mixed structure of the FM and CO microdomains [20–50 nm at 120 K$\leqslant T_C=$(140 K)] in 3% Cr-doped manganites, $Nd_{1/2}Ca_{1/2}(Mn_{0.97}Cr_{0.03})O_3$, as well as the suppressed ferromagnetic magnetization curve.

Thus, the magnetization measurement is one of the sensitive probes for detecting a coexisting ferromagnetic component. Figure 3(a) shows the M-H curve at 10 K for $(La_{1-z}Nd_z)_{1/2}Ca_{1/2}MnO_3$ ($x=0.5$). Similar to the case of $z=0.0$, the magnetization curves at $z=0.25$ and 0.50 are fairly suppressed: the ferromagnetic components are $\sim 0.5\mu_B$ (20–30 % of the ideal value). By contrast, the curve for $Nd_{1/2}Ca_{1/2}MnO_3$ ($z=1.0$) increases linearly with the applied magnetic field, reflecting the *purely* CO state.

B. Competition between CO and FM states

Here, let us see the competition between the FM and CO phases in the electronic phase diagram [Fig. 4(a)] at $x=0.45$. The middle panel [Fig. 4(b)] shows temperature variation of M measured under a field of $\mu_0 H=1.0$ T after

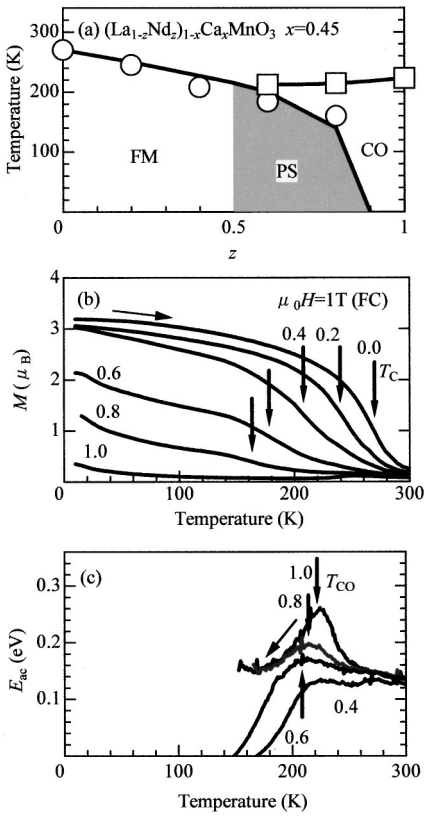

FIG. 4. (a) Electronic phase diagram, (b) magnetization M, and (c) activation energy E_{ac} for $(La_{1-z}Nd_z)_{0.55}Ca_{0.45}MnO_3$ ($x=0.45$). FM, PS, and CO represent the ferromagnetic metallic, phase separation and charge-ordered insulating states, respectively. The arrows in (b) and (c) stand for the Curie temperature T_C and the charge-ordering temperature T_{CO}, respectively. M was measured after cooling down to 5 K in the field of 1 T (FC). E_{ac} is defined by $d\ln(\rho)/d(1/T)$, where ρ is resistivity.

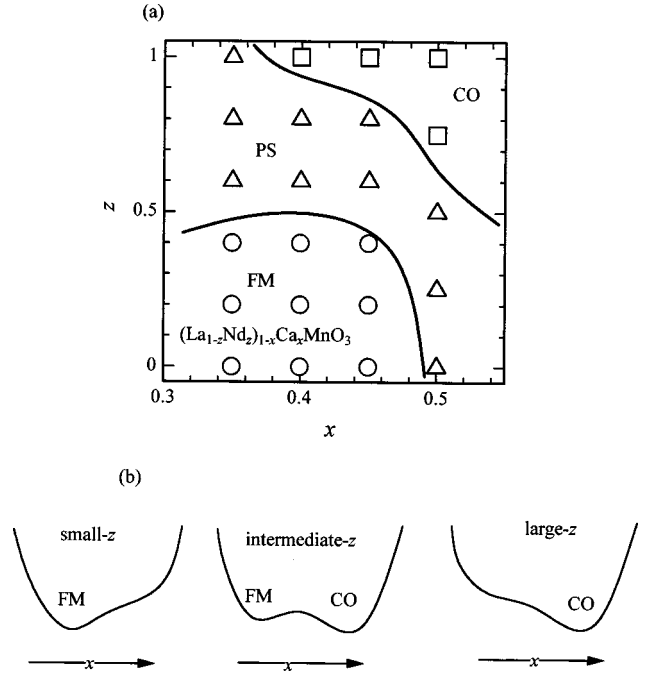

FIG. 5. Ground-state phase diagram for $(La_{1-z}Nd_z)_{1-x}Ca_xMnO_3$ against the nominal hole concentration x and Nd concentration z. The circles, triangles, and squares stand for the ferromagnetic metallic (FM), phase separation (PS), and charge-ordering insulating (CO) states, respectively. (b) A schematic picture of the total free energy against x.

cooling down to 5 K in the field (FC). T_C was tentatively determined from the inflection point of the M-T curves, and was plotted as open circles in Fig. 4(a). The M-T curve for $z \leqslant 0.4$ steeply rises below T_C (downward arrows), while the rise is rather suppressed at $z=0.6$ and 0.8. In $Nd_{0.55}Ca_{0.45}MnO_3$ ($z=1.0$), a clear cusp structure is observed in the M-T curve at $\sim$240 K, indicating an antiferromagnetic transition. To precisely determine T_{CO}, we plotted in Fig. 4(c) temperature variation of activation energy E_{ac} [$\equiv d\ln(\rho)/d(1/T)$]. T_{CO} was defined as the temperature where the E_{ac} value becomes maximum, and plotted as open squares in Fig. 4(a). A trace of the charge-ordering transition (arrows) is discernible above $z=0.6$.

The above-mentioned crossover behavior from the FM to CO state can be seen also in the M-H curves. Figure 3(b) shows the M-H curves at 10 K for $(La_{1-z}Nd_z)_{0.55}Ca_{0.45}MnO_3$ ($x=0.45$). The curves at $z=0.0$, 0.2, and 0.4 rapidly increase with magnetic field and reach $\sim 3\mu_B$ at $\sim$1 T, reflecting the *purely* FM phase. On the other hand, the curve at $z=1.0$ increases linearly with the applied magnetic field, indicating a *purely* antiferromagnetic CO state.[19] In the intermediate z region, that is, $z=0.6$ and 0.8, an incomplete ferromagnetic behavior is observed: the ferromagnetic components are $\sim 1.6\mu_B$ (50–60 % of the ideal value) and $\sim 0.7\mu_B$ (20–30 %) for $z=0.6$ and 0.8, respectively. Such a magnetization behavior indicates coexistence of the antiferromagnetic CO domains in the FM state, or the PS, similarly to the case of $La_{1/2}Ca_{1/2}MnO_3$. Thus, the PS effect [hatched region in Fig. 4(a)] is enhanced in the vicinity of the FM-CO phase boundary, where the adjacent two phases strongly compete.

C. Phase diagram

Now, let us adopt the above-mentioned procedure toward the lower-x region. Figures 3(c) and (d) show the M-H curve at 10 K for the $x=0.40$ and $x=0.35$ systems, respectively. In both the systems, the M-H curves at $z=0.0$ and 0.2 rapidly rise with field, and reach $\sim 3.5\mu_B$, reflecting the *purely* FM phase. The M-H curve, however, is gradually suppressed with further increase of z. The PS state is tentatively defined as the parameter region whose M value at $\mu_0H=1.0$ T is between 0.5 and $2.5\mu_B$, i.e., $(x,z)=(0.40,0.6)$, (0.40,0.8), (0.35,0.6), (0.35,0.8), and (0.35,1.0). We summarize in Fig. 5(a) the obtained FM (open circles), PS (open triangles), and CO (open squares) states.

Our phase diagram is consistent with the work by Ibarra *et al.*:[11] they have performed a neutron-diffraction experiment on $(La_{0.5}Nd_{0.5})_{2/3}Ca_{1/3}MnO_3$ [$(x,z)=(0.33,0.5)$], and have confirmed the coexistence of antiferromagnetic CO component in the FM phase. In addition, Yoshizawa *et al.*[20] have performed a neutron-scattering experiment on $Pr_{0.65}(Ca_{0.7}Sr_{0.3})_{0.35}MnO_3$ ($x=0.35$; z corresponds to ~ 0.5) single crystal near the FM-CO phase boundary, and have observed the coexistence of the FM and CO components in the FM phase. Arulraj *et al.*[21] have observed a reentrant transition from the CO to FM states for

$(Nd_{0.5}La_{0.5})_{0.5}Ca_{0.5}MnO_3$ $[(x,z)=(0.5,0.5)]$ near the PS-FM phase boundary. On the other hand, Zhou *et al.*[22] have reported anomalous pressure dependence of resistivity and thermopower for $(x,z)=(0.3,0.75)$, and have ascribed it to strong electron-phonon coupling. Effect of the PS, however, should be considered, since their sample locates in the PS region.

D. Lattice effects on the CO state

Finally, let us return to the structural feature on the competition between the FM and CO states. In Fig. 1 are also plotted the relative lattice constant of c against a and b, i.e., $\sqrt{2}c/(a+b)$ (filled circles), which is a crude measure of the tetragonalicity. We have found a close interrelation between the lattice structure and the stability of the CO state, that is, the smaller the relative c value becomes, the more stable the CO state is. For example, the relative c value at $x=0.35$ steeply decreases above $z=0.6$, where the CO phases appear [see Fig. 1(d)]. In addition, the reduced W in the large-z region is also advantageous for the carrier-localized CO state.

The former lattice effect seems to be essential in understanding the chemical pressure effect of Sr-based manganites. Kuwahara *et al.*[23] have derived an electronic phase diagram for $(Nd_{1-y}Sm_y)_{1/2}Sr_{1/2}MnO_3$ $(x=1/2)$, and have found that both the FM and CO phases are suppressed with decrease of the averaged radius of the perovskite A site (increase of Sm concentration y). Here, we should recall that the enhanced $\sqrt{2}c/(a+b)$ value in the large-y region (see Fig. 1 of Ref. 23) unstabilizes the CO state, even though the reduced W favors the state. Thus, the chemical pressure has two effects, i.e., bandwidth control and tetragonalicity control, at least on the charge-ordering transition.

IV. CONCLUSION

We have derived a ground-state phase diagram for filling- and structure-controlled manganites. We have found that the electronic phase separation (PS) is dominated in a wide x-z parameter region around the FM-CO phase boundary. Phenomenologically, the phase diagram is understood as follows. In the small-z (large-z) region, the total free energy of the charge-spin-orbital coupled system has one local minimum near the nominal x value which corresponds to the FM (CO) state [see schema in Fig. 5(b)]. The free energy is deformed into a double-well type in the intermediate-z region, which causes the PS as observed.[24] In order to understand the varieties of magnetotransport properties, including the global phase diagram, of the doped manganites, comprehension of the PS effect, a detailed structural analysis based on the synchrotron-radiation x-ray as well as neutron experiments should be important. We are planning such experiments to clarify the dynamical nature of the PS.

The authors are grateful to S. Mori and N. Yamamoto for fruitful discussions. This work was supported by a Grant-In-Aid for Scientific Research from the Ministry of Education, Science, Sports and Culture and from Precursory Research for Embryonic Science and Technology (PRESTO), Japan Science and Technology Corporation (JST).

[1] P. W. Anderson and H. Hasagawa, Phys. Rev. **100**, 675 (1955).
[2] P.-G. de Gennes, Phys. Rev. **118**, 141 (1960).
[3] N. Furukawa, J. Phys. Soc. Jpn. **63**, 3214 (1994); **64**, 2734 (1995); **64**, 2754 (1995); **64**, 3164 (1995).
[4] A. J. Millis, P. B. Littlewood, and B. J. Shrainman, Phys. Rev. Lett. **74**, 5144 (1995).
[5] S. Yunoki, J. Hu, A. L. Malvezzi, A. Moreo, N. Furukawa, and E. Dagotto, Phys. Rev. Lett. **80**, 845 (1998); S. Yunoki, A. Moreo, and E. Dagotto, *ibid.* **81**, 5612 (1998).
[6] G. Allodi, R. de Renzi, F. Licci, and M. W. Pieper, Phys. Rev. Lett. **81**, 4736 (1998).
[7] S. Mori, C. H. Chen, and S.-W. Cheong, Phys. Rev. Lett. **81**, 3972 (1998).
[8] P. Schiffer, A. P. Ramirez, W. Bao, and S.-W. Cheong, Phys. Rev. Lett. **75**, 3336 (1995).
[9] M. Roy, J. F. Mitchell, A. P. Ramirez, and P. Schiffer, Phys. Rev. B **58**, 5185 (1998).
[10] R. Mahendiran, R. Mahesh, R. Gundakaram, A. K. Raychudhuri, and C. N. R. Rao, J. Phys.: Condens. Matter **8**, L455 (1995).
[11] M. R. Ibarra, Guo-meng Zhao, Z. Arnold, C. Marquina, P. A. Algarabel, H. Keller, and C. Ritter, Phys. Rev. B **57**, 7446 (1998).
[12] H. J. Liu, S. L. Cooper, and S.-W. Cheong, Phys. Rev. Lett. **81**, 4684 (1998).
[13] Y. Moritomo, H. Kuwahara, Y. Tomioka, and Y. Tokura, Phys. Rev. B **55**, 7549 (1997).
[14] E. O. Wollan and W. C. Koehler, Phys. Rev. **100**, 545 (1955).
[15] P. G. Radaelli, G. Iannonce, G. Marezio, H.-Y. Hwang, S.-W. Cheong, J. D. Jorgensen, and D. N. Argyriou, Phys. Rev. B **56**, 8265 (1997).
[16] F. Izumi, in *The Rietveld Method*, edited by R. A. Young (Oxford University Press, Oxford, 1993), Chap. 13; Y.-I. Kim and F. Izumi, J. Ceram. Soc. Jpn. **102**, 401 (1994).
[17] P. Calvani, G. De Marzi, P. Dore, S. Lupi, P. Maselli, F. D'Amore, S. Gagliardi, and S.-W. Cheong, Phys. Rev. Lett. **81**, 4504 (1998).
[18] Y. Moritomo, A. Machida, S. Mori, N. Yamamoto, and A. Nakamura, Phys. Rev. B **60**, 9220 (1999).
[19] M. Tokunaga, N. Miura, Y. Tomioko, and Y. Tokura, Phys. Rev. B **57**, 5259 (1998).
[20] H. Yoshizawa, R. Kajimoto, H. Kawano, and Y. Tomoika, Phys. Rev. B **55**, 2729 (1997).
[21] A. Arulraj, A. Biswas, A. K. Raychaudhuri, C. N. R. Rao, P. M. Woodward, T. Vogt, D. E. Cox, and A. K. Cheetham, Phys. Rev. B **57**, R8115 (1998).
[22] J.-S. Zhou, W. Archibald, and J. B. Goodenough, Nature (London) **381**, 770 (1996).
[23] H. Kuwahara Y. Moritomo, Y. Tomioka, A. Asamitsu, M. Kasai, R. Kumai, and Y. Tokura, Phys. Rev. B **56**, 9386 (1997).
[24] S. Okamoto, S. Ishihara, and S. Maekawa, cond-mat/9902266 (unpublished).